Korean J. Chem. Eng., 35(5), 1073-1082 (2018)
DOI: 10.1007/s11814-018-0006-z

pISSN: 0256-1115
eISSN: 1975-7220

Hydrodynamics and design of gas distributor in large-scale amine absorbers using computational fluid dynamics

Hung Hai Pham*, Young-Il Lim*,†, Sungu Han, Bosup Lim***, and Hyun-Shin Ko****

*CoSPE, Department of Chemical Engineering, Hankyong National University, Jungang-ro 327, Anseong-si, Gyeonggi-do 17579, Korea
**Daelim, D Tower, 17 Jongno 3-gil Jongno-gu, Seoul 03155, Korea
***TPT Pacific, 19 Sannam-gil, Onsan-eup, Ulju-gun, Ulsan 45010, Korea
(*Received 4 September 2017 • accepted 11 January 2018*)

Abstract−A gas phase three-dimensional (3D) computational fluid dynamics (CFD) model was developed to investigate the hydrodynamics of gas distributors used in an amine absorber with a diameter of 3.2 m. A standard gas inlet, tubular injectors with short, medium and long lengths, and a Schoepentoeter were considered as feed systems of the gas distributors. The pressure drop, dead-area ratio and coefficient of distribution at the packing entry were used as the performance indexes of the gas distributors. The down-pipe as a liquid collector exhibited a lower dead-area ratio when compared with that of the down-comer. The tubular gas injector with a short length reduced the dead-area ratio and the gas maldistribution. The Schoepentoeter was associated with the lowest pressure drop, dead-area ratio, and coefficient of distribution among the gas distributors. The uniformity of gas distribution was enhanced by 25% in the Schoepentoeter when compared to that of the tubular gas injector.

Keywords: Power Plant, Amine Absorber, Gas Distributor, Schoepentoeter, Computational Fluid Dynamics (CFD)

INTRODUCTION

Post combustion CO_2 capture is used to treat flue gas emitted from thermal combustion units such as power plants [1]. Amine-based absorption is often adopted for CO_2 capture in large-scale power plants [2-4]. Columns packed with packing materials are employed to promote direct contact between liquid and gas phases in the absorption process [5]. Optimal operation of the packed columns requires homogeneous distribution of liquid films and gas flow [6,7]. Gas-liquid contacting devices, such as amine absorber and distillation column, include several internals such as a liquid distributor at the top, liquid collectors/redistributors, and a gas distributor at the bottom [8].

Liquid collectors are designed to collect liquid without significant interference with the upcoming gas flow [9]. The collector with a chimney tray aids in reducing the maldistribution induced by the feed system [9]. Previous studies examined several gas injection systems, including standard inlet, orifice baffle, tubular injector, horn-type distributor, and Schoepentoeter [6], which are typically used as gas distributors in packed columns. The selection of a gas distributor requires characterization and quantification of the quality of the gas flow distribution.

An area-averaged coefficient of variation (C_V) has been commonly used as an indicator of gas maldistribution induced by column internals [6,10-15]. Olujić et al. [9] used the ratio of C_V to C_M as the maldistribution index (MI) in which C_M denotes the coefficient of variance based on a local mean velocity [9]. Although the MI contains a spatial variation of the gas velocity, it tends to be sensitive to the resolution of the statistical analysis [6]. The C_V represents the magnitude of distribution although all spatial information is lost [16]. Stemich and Spiegel [16] used the coefficient of distribution (C_D) to consider both the variation magnitude and spatial distribution of gas, and applied it to a large-scale gas distributor with and without a chimney tray [16]. Petrova et al. [7] used various indexes (e.g., Coriolis coefficient, mean dynamic pressure, C_V, MI, and C_D) to experimentally evaluate the maldistribution of gas flow in absorption columns in which MI and C_D accounted for the clusters formation of gas velocity [7].

The Schoepentoeter was used for gas-liquid separation as well as an even distribution of inlet flow in strippers, absorbers and distillation columns [17]. This is a vane-type feed inlet device that distributes vapor in the gas compartment of the column by slicing up the feed gas into a series of flat jets in a smooth and uniform manner. The Schoepentoeter allows a smaller feed entry section of the column and reduces column height and cost [17].

Within the last decade, CFD has reached a significant level of maturity so that it is now considered as an indispensable analysis and design tool in a wide range of industrial applications [17]. Specifically, CFD is frequently used as a tool to design and evaluate the performance of column internals [6,9,16,18-20]. With respect to a gas distributor of bubble column, the effects of opening area, hole diameter, inlet nozzle size and its location were investigated by using an Eulerian CFD model [13]. Zarei et al. [20] examined the effect of the riser height of a conical cap tray on gas distribution in a distillation column, using Eulerian CFD with a shear stress transport turbulence model [20].

†To whom correspondence should be addressed.
E-mail: limyi@hknu.ac.kr

The CFD simulations have been often used to estimate process performance, creating appropriate performance indexes obtained from primary CFD results [6,17,21-24]. Ngo et al. [22] used an area-averaged uniformity index of a solid distribution in the CFD study of a fluidized bed with a nozzle-type gas distributor [22]. A radial non-uniformity index (RNI) defined by a normalized standard deviation for cross-sectionally averaged voidage was applied to investigate the effect of the feedstock injection angle in two-fluid CFD simulations of a fluidized-bed riser [21]. An area-averaged uniformity index of temperature (UI_T) was calculated to examine the temperature distribution of fiber tows in a low temperature carbonization furnace for carbon fiber production [24]. The uniformity index for the velocity (UI_v) was used to calculate the uniformity of resin impregnation in a carbon fiber prepreg die [23]. The high uniformity of the vertical gas velocity over the horizontal plane was confirmed for Schoepentoeter by CFD [17]. Wehrli et al. [6] investigated the effects of vapor feed systems (standard inlet, orifice baffle, tangential inlet device, tubular injector and Schoepentoeter) on the C_V of gas velocity on the horizontal plane below the packing by using CFD [6].

However, the C_V, RNI, UI_T, and UI_v cannot cover the spatial distribution for the vapor feed systems. Additionally, with the presence of chimneys, a need to investigate the influence of the vapor feed systems on gas distribution still persists with respect to various performance criteria. There also remains a need for a rigorous hydrodynamic study on the Schoepentoeter gas distributor.

In this study, we developed a three-dimensional (3D) gas phase CFD model with turbulence for gas distributors with several vapor inlet devices, such as standard gas inlet, tubular injectors with a different length, and Schoepentoeter. Three performance indexes, including the pressure drop, dead-area ratio, and coefficient of distribution for gas velocity at the packing entry, are proposed to quantify the quality of the gas flow distribution. The aim of the study involves evaluating quantitatively the performance of the vapor inlet devices by using the three indexes.

GAS DISTRIBUTOR OF AMINE ABSORBER

As shown in Table 1, six gas distributors used in an amine absorber were considered. The diameter (D) of the column was 3.2 m. Two different types of the liquid collector were applied: down-comer (Geo1) and down-pipes (Geo2). The down-comer was laid out in the right and left sides of the gas chamber (see Fig. 1(a)). Thus, the number of chimneys was six less than that of the gas distributor with the down-pipes. In Geo2 (see Fig. 1(b)), eight down-pipes were arranged on the right and left sides of the column to collect the liquid and replace the down-comer. The gas was redistributed through a chimney tray prior to reaching the packing bed. A cap with a diameter of 0.22 m was installed immediately above the spherical chimney to avoid the entry of liquid into the chimney.

The down-pipes as the liquid collector were used for the other four gas distributors as shown in Fig. 1. Short (Geo3), medium (Geo4), or long (Geo5) tubular gas injectors were installed in the gas distributor, while the Schoepentoeter was used as a gas inlet device for Geo6. The tubular gas injector included several rectangular holes oriented to the bottom. The rectangular hole size (0.68×0.35 m^2) was uniform although the number of holes was 2, 3, and 4 in Geo3, Geo4, and Geo5, respectively. The last gas distributor included the Schoepentoeter for gas injection (Geo6 in Fig. 1(f)). CFD flow fields with and without a symmetric geometry did not always agree in large-scale columns [6], and thus the CFD simulation was conducted for all the six geometries in the full domain.

The open-area ratio (=0.2), which is defined as the ratio of the total chimney hole area to the column cross-sectional area, was the same for all the geometries. The following dimensionless geometric ratios [6] were implemented on the six geometries:

$$r_{chim} = \frac{h_{chim}}{D} = 0.34$$

$$r_{sump} = \frac{h_{sump}}{D} = 0.2 \quad (1)$$

$$r_{pack} = \frac{h_{pack}}{D} = 0.22$$

where h_{chim} denotes the chimney height from the gas inlet center to the chimney, h_{sump} denotes the sump height from the bottom (or the liquid level) to the gas inlet center, and h_{pack} denotes the packing height from the chimney to the packing. r_{chim}, r_{sump}, and r_{pack} constitute the geometric ratios of the height to the column diameter (D). The liquid level was assumed to correspond to a high liquid level (HLL) of amine solution at the column bottom.

1. Operating Conditions

The flue gas passing through a quencher entered the gas distributors at 50 °C and a pressure slightly elevated from the atmosphere (approximately 1.07×10^5 Pa). The gas composition in mass was 0.7029, 0.2129, 0.0476, and 0.0366 for N_2, CO_2, H_2O, and O_2, respectively. The gas flow rate to the gas distributor was 55.318 t/h (or 25,144.8 Nm^3/h), respectively, and this was determined as 110%

Table 1. Design specification of six gas distributors

Geometry index	Column diameter (m)	Gas injection type	Liquid collector	Length (m)	Number of chimneys	Chimney hole diameter (m)
Geo1	3.2	Standard inlet	Down-comer	-	51	0.188
Geo2	3.2	Standard inlet	Down-pipe	-	57	0.188
Geo3	3.2	Tubular injector	Down-pipe	Short (1.3)	57	0.188
Geo4	3.2	Tubular injector	Down-pipe	Medium (1.8)	57	0.188
Geo5	3.2	Tubular injector	Down-pipe	Long (2.3)	57	0.188
Geo6	3.2	Schoepentoeter	Down-pipe	-	57	0.188

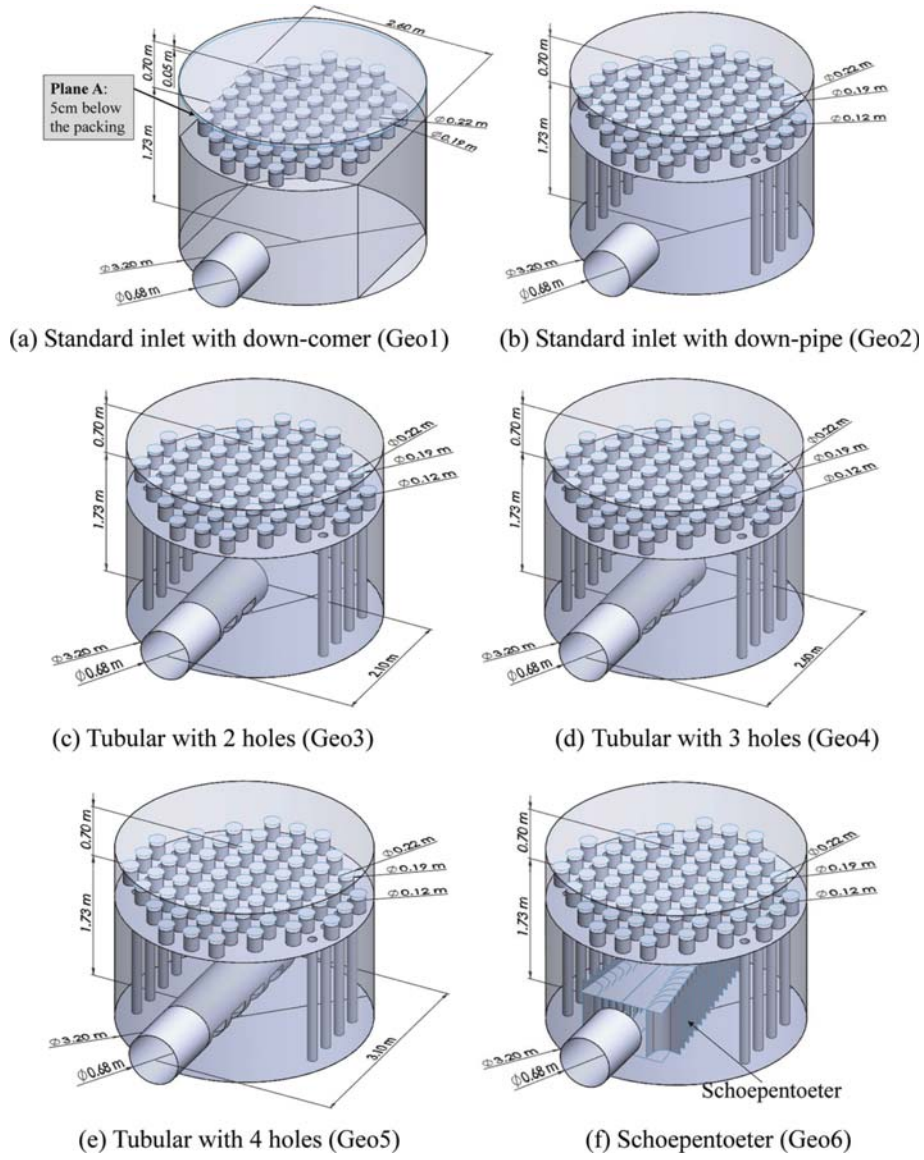

(a) Standard inlet with down-comer (Geo1) (b) Standard inlet with down-pipe (Geo2)

(c) Tubular with 2 holes (Geo3) (d) Tubular with 3 holes (Geo4)

(e) Tubular with 4 holes (Geo5) (f) Schoepentoeter (Geo6)

Fig. 1. Geometry of gas distributors with a standard gas inlet (with down-comer and down-pipe), tubular gas injectors and Schoepentoeter.

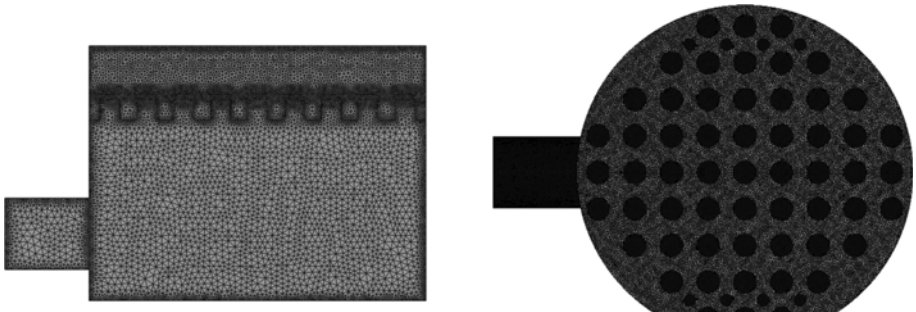

(a) Front view (b) Top view

Fig. 2. Mesh structure of a gas distributor with a standard gas inlet (Geo2).

of a normal operating condition. The gas flow rate is based on the maximum flow rate including design margin [17]. The diameters of the gas-inducing pipe corresponded to 0.68 m. Thus, the inlet gas velocity through the inducing pipe was maintained as a con-

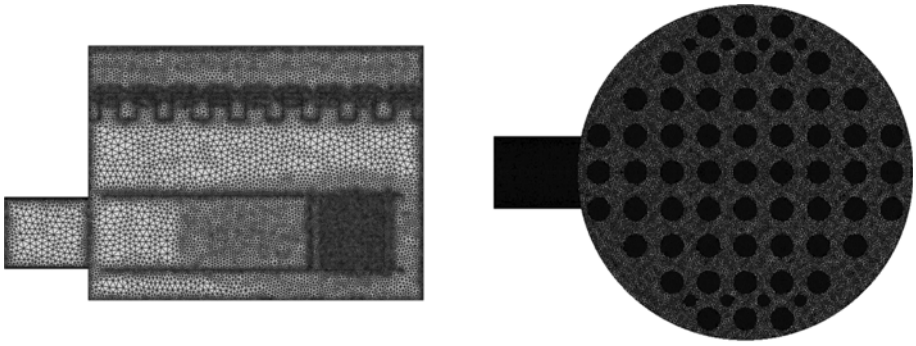

(a) Front view (b) Top view

Fig. 3. Mesh structure of a gas distributor with Schoepentoeter (Geo6).

stant at 19.2 m/s for the six cases.

2. Mesh Structure

The mesh structures are shown in Figs. 2 and 3. The polyhedral meshes were obtained from unstructured tetrahedral meshes. Fig. 2 illustrates the front and top views of the mesh structure for the gas distributor with a standard gas inlet (Geo2). The meshes are concentrated on the walls and near the chimneys to capture a high gradient of the velocity. In Fig. 3(a), the mesh density increases with the flow direction, since it is expected that the gradients of pressure and velocity increase as the inner space of Schoepentoeter decreases. The mesh structure at the top of the gas distributor is the almost same for Geo2 and Geo6 (see Fig. 2(b) and Fig. 3(b)).

A mesh independent test was conducted for Geo2. The number of polyhedral cells corresponded to 1.09 million, 1.68 million, and 3.08 million for the coarse, medium, and fine mesh structures, respectively. The number of polyhedral cells for the six full geometries used in the study was 1.64 million, 1.68 million, 1.83 million, 1.88 million, 1.95 million, and 3.24 million, respectively, depending on the resolution required to capture geometry details of the injection system. The average volume of polyhedral cells was 12.11 cm^3, 11.78 cm^3, 10.82 cm^3, 10.51 cm^3, 10.18 cm^3, and 6.21 cm^3, respectively. The gas distributor with Schoepentoeter has a relatively small mesh size because of the complex geometry of flat jets.

GAS PHASE CFD MODEL AND PERFORMANCE INDEX

A 3D steady-state CFD model was developed for the gas distributor. The gas phase was assumed as incompressible. Temperature variations were neglected. The influence of the liquid on the gas phase is small and negligible [6]. The governing equation includes the continuity and momentum conservations. A realizable k-ε model [25,26] is adopted for turbulence in the momentum equation.

1. Governing Equations

The incompressible continuity equation of the gas phase is expressed as follows:

$$\rho\vec{\nabla}\cdot\vec{u}=0 \tag{2}$$

where ρ denotes the gas density, and $\vec{u}$ denotes the gas velocity vector.

The momentum equation of fluid at a steady-state results in the following equation:

$$\rho\vec{\nabla}\cdot(\vec{u}\vec{u})=-\vec{\nabla}P+\vec{\nabla}\cdot(\bar{\bar{\tau}}_t)+\rho\vec{g} \tag{3}$$

where P denotes the static pressure, and $\rho\vec{g}$ denotes the gravitational force. The stress tensor ($\bar{\bar{\tau}}_t$) for turbulence is given by the following expression:

$$\bar{\bar{\tau}}_t=(\mu+\mu_t)\left[(\vec{\nabla}\vec{u}-(\vec{\nabla}\vec{u})^T)-\frac{2}{3}\vec{\nabla}\cdot\vec{u}\bar{\bar{I}}\right]-\frac{2}{3}\rho k\bar{\bar{I}} \tag{4}$$

where $\bar{\bar{I}}$ denotes the identity tensor, and $(\nabla\vec{u}-(\nabla\vec{u})^T)$ denotes the strain rate. Additionally, μ denotes the molecular viscosity. μ_t denotes the turbulence viscosity, and this is computed as a function of k and ε in the turbulence model.

2. Turbulence Model

A turbulent flow is characterized by fluctuating velocity fields due to complex geometry and/or high velocity. A turbulent flow is modeled by using a realizable k-ε equation, which includes a new formulation for turbulent viscosity (μ_t) and a new transport equation for the dissipation rate (ε) [25]. The turbulence equation represents the transport of the turbulence kinetic energy (k) and its dissipation rate (ε). At the steady-state, the realizable k-ε model is expressed as follows:

$$\begin{aligned}
&\rho\vec{\nabla}\cdot(\vec{u}k)=\vec{\nabla}\cdot\left[\left(\mu+\frac{\mu_t}{\sigma_k}\right)\vec{\nabla}k\right]-G_k-\rho\varepsilon\\
&\rho\vec{\nabla}\cdot(\vec{u}\varepsilon)=\vec{\nabla}\cdot\left[\left(\mu+\frac{\mu_t}{\sigma_\varepsilon}\right)\vec{\nabla}\varepsilon\right]+\rho C_1 S\varepsilon-\rho C_2\frac{\varepsilon^2}{k+\sqrt{v\varepsilon}}\\
&\mu_t=\rho C_\mu\frac{k^2}{\varepsilon},\ C_1=\max\left[0.43,\frac{\eta}{\eta+5}\right],\ \eta=S\frac{k}{\varepsilon},\\
&S=\sqrt{2S_{ij}S_{ij}},\ S_{ij}=\frac{1}{2}\left(\frac{\partial u_j}{\partial x_i}+\frac{\partial u_i}{\partial x_j}\right)\\
&C_\mu=\frac{1}{A_0+A_s\frac{kU^*}{\varepsilon}},\ U^*=\sqrt{S_{ij}S_{ij}+\overline{\Omega}_{ij}\overline{\Omega}_{ij}}
\end{aligned} \tag{5}$$

where G_k denotes the generation of k due to the mean velocity gradient, and σ_k and σ_ε denote the turbulent Prandtl numbers of k and ε, respectively. Additionally, C_1 and C_2 denote the model coefficients of ε. The turbulent viscosity (μ_t) is computed from the k, ε, and C_μ values. The S, S_{ij}, and $\overline{\Omega}_{ij}$ denote the modulus of the mean rate of strain tensor, mean strain rate, and mean rate of the rota-

tion tensor, respectively. C_μ is a function of the mean strain and rotation rates and the angular velocities of the system rotation and the turbulence fields [25]. A_0 is the model constant, and A_s denotes the parameter as a function of S_{ij}, S_{jk}, and S_{ki}.

The realizable turbulence model was developed to capture the rotation, separation, and recirculation of flows in the 3D CFD [25]. The realizable k-ε model satisfying mathematical constraints on the Reynolds stresses differs from other k-ε models in the formulation of turbulent viscosity (μ_t) and turbulence energy dissipation rate (ε). The realizable k-ε model is suitable for complex shear flows, while the standard k-ε model is robust but valid only for fully-developed turbulent flows (ANSYS Fluent Theory Guide 17.1, ANSYS Inc., 2016).

3. Performance Index

Three indexes including the pressure drop (ΔP), dead-area ratio (χ), and coefficient of distribution (C_D) are used to describe the performance of the gas distributor and the quality of gas distribution. The ΔP between the inlet and outlet of the gas distributor is defined as follows:

$$P_{in}=\frac{\Sigma_i P_i \Delta A_{in,i}}{\Sigma_i \Delta A_{in,i}} \qquad (6)$$
$$\Delta P = P_{in} - P_{out}$$

where P_{in} is calculated from an average value of P over the inlet area (A_{in}), and P_{out} is the outlet pressure that is prescribed as a boundary condition.

The χ is calculated as follows:

$$\bar{u}_y=\frac{\Sigma_k u_{y,k} A_k}{\Sigma_k A_k}$$
$$\chi=\frac{A_{dead}}{A_c},\ A_{dead}=\Sigma_k \Delta A_k \text{ for } u_{y,k}\le 0.1\bar{u}_y \qquad (7)$$

where A_c denotes the cross-sectional area of column. A_{dead} denotes the dead area that corresponds to the sum of areas (A_k) in which the vertical gas velocity ($u_{y,k}$) is lower than 10% of the area-averaged vertical velocity ($\bar{u}_y$). The dead area is calculated by using a user-defined function (UDF) on Plane A which is 5 cm below the packing (see Fig. 1(a)). The dead-area implies a stationary area that may result in insufficient contact between gas and liquid in the column packing.

A uniform distribution of velocity across the column at the packing entry is important for gas and liquid contact in the amine absorber. The C_D that accounts for both magnitude and spatial distribution [16] is defined as follows:

$$C_D=\frac{C_V}{\phi} \qquad (8)$$

where C_V denotes the coefficient of variance [10,27], and ϕ denotes the distribution length scale. A smaller C_V, longer ϕ, and lower C_D constitute a better gas distribution.

The C_V is defined as follows:

$$\sigma_y=\sqrt{\frac{\Sigma_k (u_{y,k}-u_y)^2 A_k}{\Sigma_k A_k}}$$
$$C_V=\frac{\sigma_y}{\bar{u}_y} \qquad (9)$$

The area-averaged velocity ($\bar{u}_y$) in the vertical direction (y) was obtained on plane A (see Fig. 1(a)). The standard deviation (σ_y) was also calculated on this plane. The C_V corresponds to the ratio of the standard deviation to the mean velocity.

ϕ is defined as the ratio of the total length of the contact line (l) to a characteristic length of the system (l_{char}) as follows:

$$\left|\vec{\nabla}\vec{u}\right|=\sqrt{\Sigma_{j=x,y,z}\left[\left(\frac{\partial u_j}{\partial x}\right)^2+\left(\frac{\partial u_j}{\partial y}\right)^2+\left(\frac{\partial u_j}{\partial z}\right)^2\right]}$$
$$l=\frac{\Sigma_k \left|\vec{\nabla}\vec{u}\right|_k A_k}{2\sigma_y}$$
$$l_{char}=\frac{A_c}{D_h}=\frac{\pi D}{4} \qquad (10)$$
$$\phi=\frac{l}{l_{char}}$$

The norm of the velocity gradient ($\left|\vec{\nabla}\vec{u}\right|$) was calculated from the gradient of the three velocities in three directions (x, y, and z). The total length (l) of contact lines between two adjacent cells was scaled by dividing by $2\sigma_y$. The l_{char} was obtained by dividing the column cross-sectional area (A_c) by the hydraulic diameter (D_h), and this resulted in $\pi D/4$. The dimensionless ϕ implies the spatial distribution of flow local irregularities over a given cross-sectional area [16].

Note that C_D in Eq. (8) differs from the value obtained by Stemich and Spiegel [16] with respect to the definition of C_V in Eq. (9). The vertical velocity (u_y) was used for C_V in this study, while all three velocities were used by Stemich and Spiegel [16]. It is expected that C_V based on u_y emphasizes the maldistribution of flows in the vertical direction.

4. Boundary Conditions and Model Parameters

The inlet boundary condition was set such that it was the same as the operating condition: 55.318 t/h at T=50 °C. The outlet (or

Table 2. CFD model parameters

	Symbol		Value
Continuity equation	ρ	Gas density (kg/m^3)	1.38
Momentum equation	μ	Gas viscosity (Pa·s)	1.865×10^{-5}
Turbulence equation	I_t	Turbulence intensity of inlet velocities (%)	I_t=5
(Realizable k-ε model)	σ_k	Turbulent Prandtl number for k	σ_k=1.0
	σ_ε	Turbulent Prandtl number for ε	σ_ε=1.2
	C_2	Constant of dissipation rate (ε)	C_2=1.9
	A_0	Constant of turbulent viscosity (μ_t)	A_0=4.04

packing entry) was set as the pressure outlet with a gage pressure of P_{out}=5,400 Pa, which corresponds to the packing pressure drop. Table 2 shows the model parameters that are classified as continuity, momentum, and turbulence equations.

The calculations were performed on a workstation with 48 cores of 2.7 GHz CPU and 128 GB RAM. A SIMPLE method was selected for pressure-velocity coupling. A PRESTO scheme was used for the spatial discretization of pressure due to a high swirling flow in the gas distributor. A second order scheme was used for the spatial discretization of the other derivative terms. The CFD model was calculated by using a steady-state solver in the finite volume method. The convergence tolerance was set to 1×10^{-3}. The number of iterations varied from 2,500 to 5,600 for the six steady-state CFD simulations, which corresponded to one to three hours of the calculation time, respectively, on the workstation. The UDF for the dead-area ratio (χ) was implemented on ANSYS Fluent R17.1 (ANSYS Inc., USA, 2016).

CFD RESULTS AND DISCUSSION

A mesh independent test was conducted for the gas distributor with the standard gas inlet and the down-pipe liquid collector (Geo2). The effects of the two liquid collectors (down-comer and down-pipe) on the gas distributor (Geo1 and Geo2, respectively) with the standard gas inlet were examined. The velocity contours and the performance indexes were compared for the six gas distributors.

1. Mesh Independent Test

Coarse (1.09 million cells), medium (1.68 million cells), and fine (3.08 million cells) meshes were constructed for a standard inlet gas system with eight down-pipes (Geo2, as shown in Fig. 1(b)). The effect of the cell number (N_{cell}) was examined on the area-averaged inlet pressure (P_{in}) and the volume-averaged gas velocity (u_{avg}) in the chamber.

The inlet pressure (P_{in}) exhibits a slight change according to the cell number (N_{cell}) as shown in Fig. 4(a). The variation of P_{in} corresponds to 5,721±1 Pa. However, u_{avg} on the coarse mesh is relatively low when compared to those in the other two mesh structures (see Fig. 4(b)). The medium mesh (1.68 million cells) was selected as a compromise between accuracy and computational efficiency.

2. Standard Gas Inlet

The following two different liquid collector types were consid-

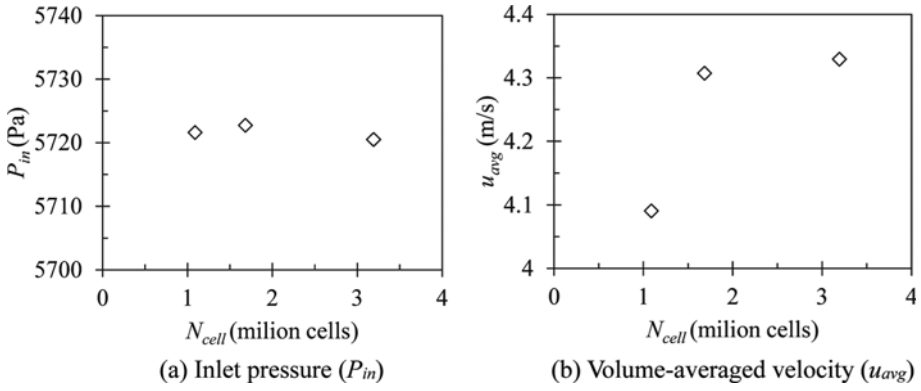

Fig. 4. Mesh independent tests for coarse, medium, and fine meshes for a gas distributor with a standard inlet and down-pipe (Geo2).

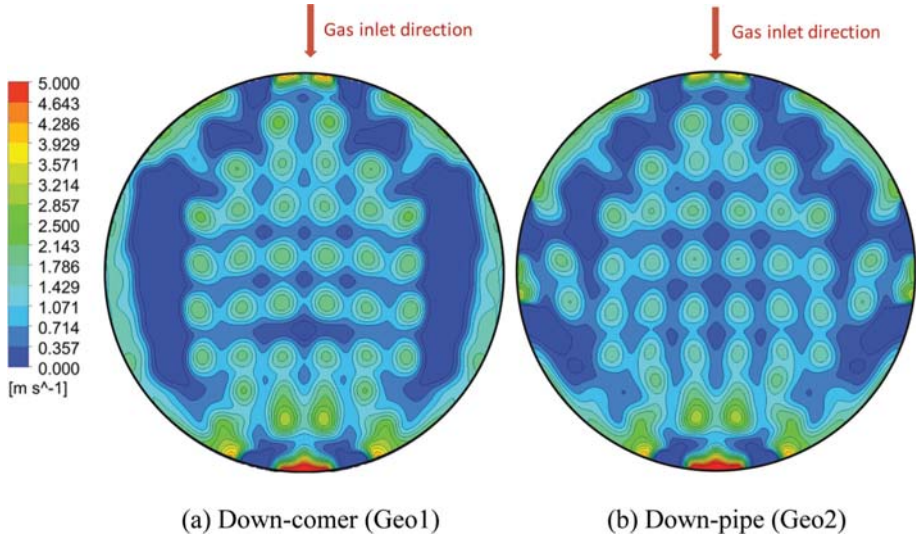

Fig. 5. Vertical velocity contour 5 cm below the packing for gas distributors with a standard inlet (top view).

ered in the gas distributor: down-comers and down-pipes. The effect of the liquid collectors on the gas distribution was investigated in the standard gas inlet and chimney tray. Fig. 5 illustrates the vertical velocity (u_y) contours on Plane A (see Fig. 1(a)) for Geo1 and Geo2.

A large low-velocity area is observed in the right and left sides of the column when the chimney tray is combined with the down-comer (see Fig. 5(a)). However, the low-velocity area reduces in the chimney tray with the down-pipe (see Fig. 5(b)). The highest velocity appears in the side opposite to the gas inlet for the standard gas inlet system.

Table 3 shows the performance indexes of the standard inlet and chimney tray gas distributors with the down-comer and down-pipe. When the down-pipe (Geo2) is used, the pressure drop (ΔP) decreases by 4.9% and the dead-area ratio (χ) significantly de-

Table 3. Performance indexes of gas distributors with a standard gas inlet (with down-comer and down-pipe), and tubular gas injectors

Performance index	Unit	Gas injection system				
		Geo1 (down-comer)	Geo2 (down-pipe)	Geo3 (2-hole)	Geo4 (3-hole)	Geo5 (4-hole)
Averaged-velocity at Plane A	m/s	0.8657	0.8658	0.8658	0.8657	0.8656
Pressure drop (ΔP)	Pa	338	322	399	322	305
Dead-area ratio (χ)	-	0.19	0.13	0.11	0.15	0.17
Coefficient of variation (C_V)	-	1.00	0.89	0.85	0.90	0.97
Length scale (ϕ)	-	2.26	2.50	2.53	2.36	2.44
Coefficient of distribution (C_D)	-	0.444	0.356	0.335	0.381	0.398

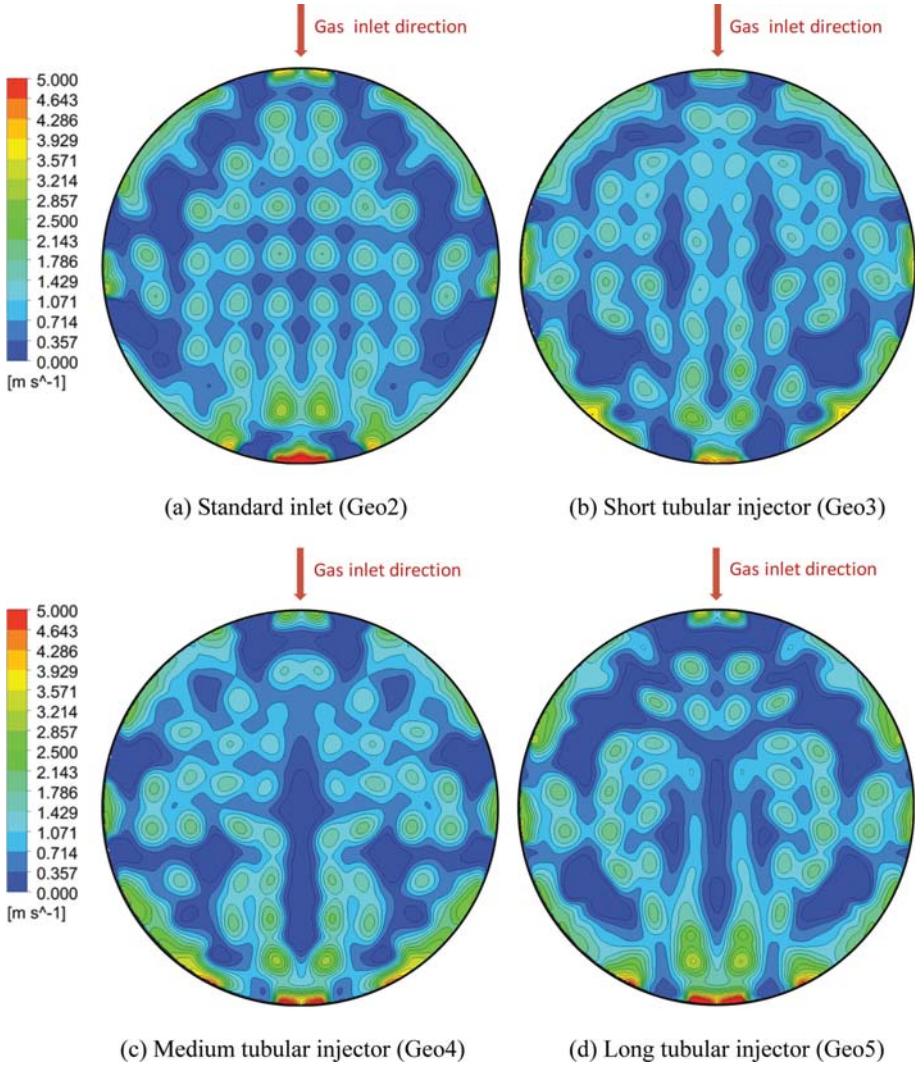

Fig. 6. Vertical velocity contour 5 cm below the packing for gas distributors with a standard inlet and tubular injector (top view).

creases, compared to the down comer (Geo1). Since the C_V reduces and the ϕ increases with the down-pipe, the C_D decreases from 0.444 to 0.356. The down-comer develops a strong dead zone near two wall sides and exhibits a high value of C_D. Therefore, the down-pipe is adopted for further investigations on the gas injection systems.

3. Tubular Gas Injectors

The gas distributor with the standard inlet (Geo2) was compared to those with the short, medium, and long tubular injectors (Geo3, Geo4, and Geo5) with 2, 3, and 4 rectangular holes, respectively. Fig. 6 depicts the vertical velocity contours of the four gas distributors on Plane A (see Fig. 1(a)). The holes of the tubular injectors are open toward the bottom and the gas flow rises from the bottom. Therefore, the flow pattern appears as split into the right and left sides. It was also observed that the longer tubular injectors do not improve the gas distribution.

The performance indexes of the three gas distributors with short, medium and long tubular (Geo3, Geo4, and Geo5) are listed in Table 3. The ΔP decreases as the open-area ratio of tubular pipe increases with increasing the number of holes. The ΔP of the standard inlet (Geo2) is the almost same as that of the long tubular injector with three holes (Geo4). The short tubular injector with two holes (Geo3) exhibits the lowest χ and C_D among the four gas distributors, albeit at the cost of a pressure drop. The standard inlet (Geo2) exhibits a lower χ and C_D than the medium and long tubular gas injectors (Geo4 and Geo5), and this implies that the opening ratio and length of the tubular injector play important roles in the gas distribution.

4. Gas Distributor with Schoepentoeter

The Schoepentoeter as a gas injection device was applied to the gas distributor to improve the gas distribution. Fig. 7 shows the pressure contour and the velocity vector in the middle of Schoepentoeter. The gas is compressed in the inner side of flat jets as shown in Fig. 7(a). A relatively uniform pressure profile is observed over the cross-sectional area. As shown in Fig. 7(b), the gas velocity decreases when it exits the Schoepentoeter because the total outlet

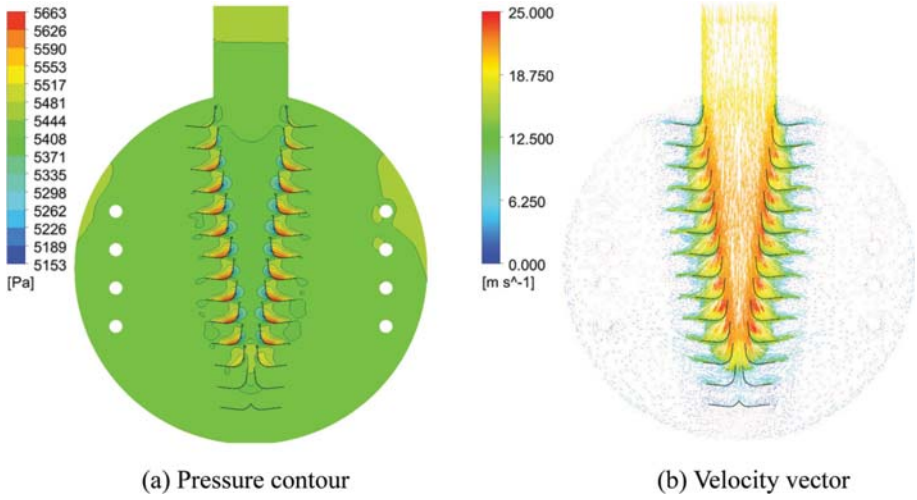

Fig. 7. Pressure contour and velocity vector in the middle of Schoepentoeter (top view).

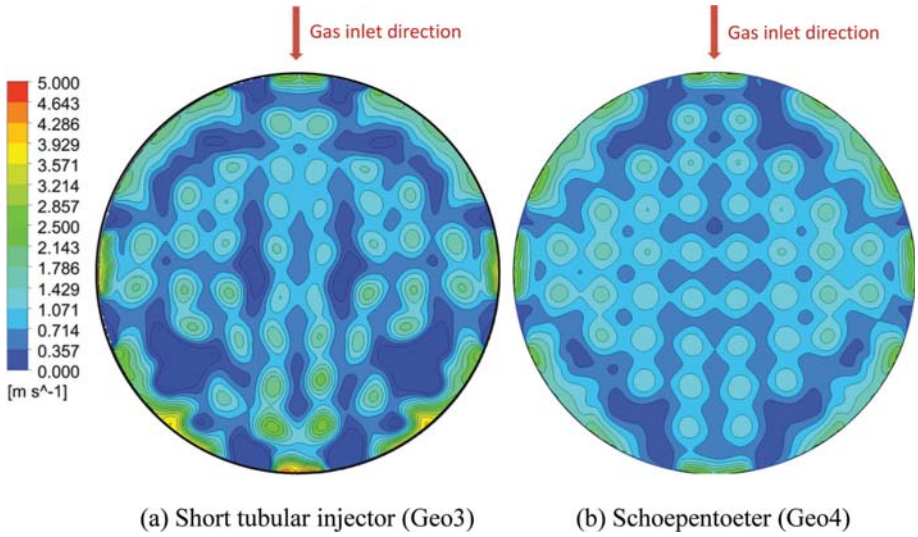

Fig. 8. Vertical velocity contour 5 cm below the packing for gas distributors with a short tubular injector and Schoepentoeter (top view).

Table 4. Difference of performance indexes between gas distributors with a short tubular injector and Schoepentoeter

Performance index	Unit	Gas injection system		Difference (%)[a]
		Geo3 (Short tubular, 2-hole)	Geo6 (Schoepentoeter)	
Averaged-velocity at Plane A	m/s	0.8658	0.8662	0.05
Pressure drop (ΔP)	Pa	399	295	−26.1
Dead-area ratio (χ)	-	0.11	0.07	−34.8
Coefficient of variation (C_V)	-	0.85	0.60	−29.0
Length scale (ϕ)	-	2.53	2.39	−5.6
Coefficient of distribution (C_D)	-	0.335	0.252	−24.8

[a]Difference=100×(tubular−Schoepentoeter)/(tubular)

area (3.92 m^2) of the Schoepentoeter significantly exceeds the inlet area (0.36 m^2). The gas flow is effectively distributed because the inner space of Schoepentoeter becomes narrow along the axial distance. Specifically, the jet length and the gap between two adjacent flat jets significantly affect the performance of Schoepentoeter.

Fig. 8 compares the velocity contours between the short tubular injector (Geo3) and Schoepentoeter (Geo6). The velocity contour of Schoepentoeter appears more uniform than that of the short tubular injector. However, a few dead areas are observed in the gas inlet and its opposite side as shown in Fig. 8.

Table 4 lists the performance indexes for the gas distributor with the short tubular injector (Geo3) and Schoepentoeter (Geo6). The gas distributor with the Schoepentoeter (Geo6) results in a substantial decrease in ΔP, χ, and C_V values. Unlike the gas distributor with the short tubular injector (Geo3), a large open-area of Schopentoeter allows smooth flow of gas. Therefore, the pressure drop of Schopentoeter is much lower than that of the gas distributor with the tubular injector (Geo3), and even lower than that of the gas distributor with the standard inlet (Geo2). It is attributed to the fact that the collision between the injecting gas flow and the opposite wall results in a pressure loss of the gas distributor (Geo2).

The distribution length scale (ϕ) does not improve when the Schoepentoeter is used. Since the norm of the velocity gradient decreases more than the standard deviation (see Eq. (10)), the length of the contact line (l) decreases from 6.37 m to 6.01 m, and ϕ reduces by 5.6%. The C_D of Schoepentoeter decreases by 24.8% due to the enhancement in C_V when compared to that of the short tubular injector.

The C_D was 0.01 above a rectangular absorber (1.441.12 m) with a standard gas inlet and random packing [7]. Stemich and Spiegel [16] reduced C_D to 0.096 by using a gas distributor (D=8.8 m) with a tangential inlet device and rectangular chimney tray [16]. The importance of a homogeneous gas distribution increases with increases in the column diameter. The three performance indexes (ΔP, χ, and C_D) provide quantitative guidelines to design large-scale gas distributors.

CONCLUSION

The role of the gas distributor is important for an even distribution of gas over the cross-sectional area when the column diameter increases. In this simulation study, a large-scale gas distributor used in an amine absorber with a diameter of 3.2 m was considered to investigate the uniformity of the gas distribution according to several gas-inducing systems, including standard gas inlet, tubular injectors, and Schoepentoeter. A spherical chimney tray was installed above the gas inlet devices. Two down-comers or eight down-pipes as a liquid collector were arranged in the two sides of the chimney tray.

An incompressible steady-state 3-dimensional (3D) computational fluid dynamics (CFD) model included the continuity, momentum, and realizable k-ε turbulence model. The pressure drop (ΔP), dead-area ratio (χ), and coefficient of distribution (C_D) were used as the performance indexes of the gas distributors. The C_D quantified both the variation magnitude and spatial distribution of the gas flow at the packing entry located above the chimney. The lower the ΔP, χ, and C_D are, the better the gas distribution.

Since the gas distributor with the down-comer exhibited higher χ and C_D values than those of the down-pipe, the chimney tray with the down-pipe was used for the other gas distributors. A tubular injector with a short length (two exit holes) exhibited lower χ and C_D than those of medium (three exit holes) and long (four exit holes) lengths at the cost of ΔP. The Schoepentoeter displayed the best performance in terms of ΔP, χ, and C_D, and these could be used as quantitative indexes to design large-scale gas distributors.

ACKNOWLEDGEMENTS

This study was supported by the Korea Institute of Energy Technology Evaluation and Planning (KETEP)-granted financial resource from the Ministry of Trade, Industry & Energy, Republic of Korea (No. 20142010201810). This study was also funded by the Basic Science Research Program through the National Research Foundation of Korea (NRF) of the Ministry of Science, ICT, and future Planning (Grant number: NRF-2016R1A2B4010423).

NOMENCLATURE

A : cross-sectional area [m^2]
A_0 : model constant of turbulence viscosity
A_c : cross-sectional area of a column [m^2]
A_{dead} : dead area where gas velocity is less than 0.1 m/s [m^2]
A_{in} : cross-sectional area of a gas inlet pipe [m^2]
A_s : parameter of turbulence viscosity

C_1, C_2 : parameters of turbulent dissipation rate
C_D : coefficient of distribution
C_V : coefficient of variance
C_m : parameter of turbulence viscosity
D : column diameter [m]
D_h : hydraulic diameter [m]
g : gravitational acceleration [m s^{-2}]
G_k : generation of turbulent kinetic energy [kg $m^{-1}s^{-3}$]
h_{chim} : height from gas inlet to chimney [m]
h_{pack} : height from chimney to packing [m]
h_{sump} : height from bottom to gas inlet [m]
$\bar{\bar{I}}$: identity tensor [kg m^{-1}]
I_t : turbulent intensity [%]
k : turbulence kinetic energy [m^2s^{-2}]
l : length of contact line [m]
l_{char} : characteristic length [m]
N_{cell} : total number of cells
P : pressure [Pa]
P_{in} : inlet pressure [Pa]
P_{out} : outlet pressure [Pa]
Q_{gas} : total mass flow rate of gas [kg/s]
r_{chim} : geometric ratio of chimney height to column diameter
r_{pack} : geometric ratio of packing height to column diameter
r_{sump} : geometric ratio of sump height to column diameter
S : modulus of mean rate of strain tensor [s^{-1}]
S_{ij} : mean strain rate [s^{-1}]
$\vec{u}$: gas velocity [ms^{-1}]
u_{avg} : average gas velocity [ms^{-1}]
u_y : vertical gas velocity [ms^{-1}]
U^* : parameter of turbulence viscosity [s^{-1}]
V : volume [m^3]
x : spatial direction length [m]
y : gravity direction length [m]
z : spatial direction length [m]

Greek Letters

χ : dead-area ratio
ΔP : pressure drop [Pa]
ε : dissipation rate of k [m^2s^{-3}]
ϕ : distribution length scale
η : mean strain
μ : viscosity [Pa·s]
μ_t : turbulent viscosity [Pa·s]
ρ : density [kgm^{-3}]
σ_k : turbulent Prandtl number of k
σ_ε : turbulent Prandtl number of ε
σ_y : standard deviation of vertical velocity [ms^{-1}]
$\bar{\bar{\tau}}$: stress tensor [kg m^{-2} s^{-2}]
$\overline{\Omega_{ij}}$: mean rate of rotation tensor [s^{-1}]

REFERENCES

1. M. K. Mondal, H. K. Balsora and P. Varshney, *Energy*, **46**, 431 (2012).
2. M. Wang, A. Lawal, P. Stephenson, J. Sidders and C. Ramshaw, *Chem. Eng. Res. Des.*, **89**, 1609 (2011).
3. J. H. Lee, N. S. Kwak, I. Y. Lee, K. R. Jang, D. W. Lee, S. G. Jang, B. K. kim and J.-G. Shim, *Korean J. Chem. Eng.*, **32**, 800 (2015).
4. M. Zaman and J. H. Lee, *Korean J. Chem. Eng.*, **30**, 1497 (2013).
5. A. Aroonwilas, A. Chakma, P. Tontiwachwuthikul and A. Veawab, *Chem. Eng. Sci.*, **58**, 4037 (2003).
6. M. Wehrli, S. Hirschberg and R. Schweizer, *Chem. Eng. Res. Des.*, **81**, 116 (2003).
7. T. Petrova, N. Vaklieva-Bancheva, S. Darakchiev and R. Popov, *Clean Technol. Environ.*, **16**, 1381 (2014).
8. A. Gorak and Z. Olujic, *Distillation: Equipment and Processes*, Academic Press, London (2014).
9. Ž. Olujić, A. Mohamed Ali and P. J. Jansens, *Chem. Eng. Process.*, **43**, 465 (2004).
10. J. F. Billingham, D. P. Bonaquist and M. J. Lockett, *Institution of Chemical Engineers Symposium Series*, **142**, 841 (1997).
11. M. T. Dhotre and J. B. Joshi, *Can. J. Chem. Eng.*, **81**, 677 (2003).
12. T. Petrova, K. Semkov and C. Dodev, *Chem. Eng. Process.*, **42**, 931 (2003).
13. M. T. Dhotre and J. B. Joshi, *Chem. Eng. J.*, **125**, 149 (2007).
14. D. P. Edwards, K. R. Krishnamurthy and R. W. Potthoff, *Chem. Eng. Res. Des.*, **77**, 656 (1999).
15. R. Darakchiev and C. Dodev, *Chem. Eng. Process.*, **41**, 385 (2002).
16. C. Stemich and L. Spiegel, *Chem. Eng. Res. Des.*, **89**, 1392 (2011).
17. G. Mosca, P. Schaeffer and B. Griepsma, *Sulzer Technical Review*, **3**, 6 (2010).
18. J. Kim, D. A. Pham and Y.-I. Lim, *Chem. Eng. Res. Des.*, **121**, 99 (2017).
19. A. Mohamed Ali, P. J. Jansens and Ž. Olujić, *Chem. Eng. Res. Des.*, **81**, 108 (2003).
20. T. Zarei, E. Abedini, R. Rahimi and J. Khorshidi, *Korean J. Chem. Eng.*, **34**, 969 (2017).
21. S. Chen, Y. Fan, Z. Yan, W. Wang, X. Liu and C. Lu, *Chem. Eng. Sci.*, **153**, 58 (2016).
22. S. I. Ngo, Y.-I. Lim, B.-H. Song, U.-D. Lee, J.-W. Lee and J.-H. Song, *Powder Technol.*, **275**, 188 (2015).
23. S. I. Ngo, Y.-I. Lim, M.-H. Hahn, J. Jung and Y.-H. Bang, *Comput. Chem. Eng.*, **103**, 58 (2017).
24. H. H. Pham, Y.-i. Lim, C.-H. Cho and Y.-H. Bang, *Chem. Eng. Res. Des.*, **128**, 192 (2017).
25. T. H. Shih, W. W. Liou, A. Shabbir, Z. Yang and J. Zhu, *Comput. Fluids*, **24**, 227 (1995).
26. M. I. Kim, Y. Lee, B. W. Kim, D. H. Lee and W. S. Song, *Korean J. Chem. Eng.*, **26**, 359 (2009).
27. Ž. Olujić, *Chinese J. Chem. Eng.*, **19**, 726 (2011).